Efficient optimisation of large aircraft fuselage structures

W. J. Vankan and R. Maas
vankan@nlr.nl
Aerospace Vehicles Division
National Aerospace Laboratory NLR
Amsterdam
The Netherlands

S. Grihon
Airbus
Toulouse
France

ABSTRACT

This paper presents an innovative optimisation method for aircraft fuselage structural design. Detailed local finite element analyses of panel buckling are further processed such that they can be applied as failure constraints in the global level optimisation. The high computational costs involved with the finite element analyses are limited by advanced use of surrogate modelling methods. This yields high flexibility and efficiency in the local level optimisation procedure and allows for efficient gradient based search methods as well as more costly direct search optimisations like genetic algorithms (GAs). The method is demonstrated on a composite fuselage barrel design case considering common structural sizing variables like thicknesses and stringer dimensions. Optimised barrel designs are obtained where the constraints that are derived from the panel buckling analyses are active. The total computational cost for the complete local and global level optimisation procedures is in the order of days on common-performance hardware.

1.0 INTRODUCTION

International competition urges aeronautic industry to continuously enhance its performance in the engineering design process. The application of innovative design methods and novel materials is of key importance for the further reduction of design time and increased design confidence level. On the materials side, carbon composite materials are being used more and more on commercial aircraft, up to more than 50% of the structural weight of current state of the art aircraft like the

Paper No. 3983. Manuscript received 23 March 2013, first revised version received 6 August 2013, second revised version received 12 October 2013, accepted 15 October 2013.
A version of this paper appeared at the 3rd Aircraft Structural Design Conference in Delft, The Netherlands, October 2012.

https://doi.org/10.1017/S0001924000008915 Published online by Cambridge University Press

Boeing B787 and the Airbus A350[1]. Composite materials have several advantages compared to metallic materials, such as higher ratios of stiffness and strength to density, less progressive damage under in-service fatigue and lower sensitivity to corrosion[1]. On the design methods side, fast and accurate design analyses and optimisation methods are a prerequisite to identify the most beneficial design options and to achieve optimised local sizing of structural components. But the design of large structures like aircraft fuselages requires a variety of tools and methods, including computationally expensive analyses, to accurately assess the typical failure modes for weight optimised design, like local buckling[2]. Therefore the design of such structures is usually performed by analyses and optimisations on different levels (e.g. see Ref. 3): relatively simple analyses and optimisations on the global fuselage barrel level and more detailed analyses and optimisations on the local level of a single stiffened skin bay[2]. The aim of the study behind this paper is to develop new design methods for computationally efficient optimisation of aircraft fuselage structures.

An early implementation of a design optimisation method for fuselage structures considering multiple levels was presented in Ref. 4. This method considered structural modelling on two levels of detail: a so-called lumped finite element (FE) model for the over-all stress and deflection analysis and refined models based on handbook formulas for detailed design and constraint evaluation of frames and stringer cross sections and skin thicknesses. Although quite computationally efficient, this implementation was also quite specific to the considered application (e.g. z-stringers, I and C frames).

Various multi-level optimisation methodologies were developed for multi-disciplinary design and optimisation of aircraft. In general these methodologies considered algorithms for the multi-level decomposition of the multi-disciplinary design problem and the coordination of the evolving multiple coupled optimisation problems in computational frameworks. Co-ordination methods for decomposed optimisation problems initially focussed on linearising the coupling between the problems in the hierarchy. The problem on the top-levels prescribes the necessary coupling parameters to the problems at the lower level. The lower levels provide the top-level with sensitivity data on the behaviour under various coupling conditions. Early implementations of such decomposition-coordination methods for multi-level optimisation were proposed in Refs 5, 6 and 7, amongst others. The need for optimum sensitivity analysis in order to provide additional information to other parts of the decomposed optimisation problem was published in Ref. 8. Research showed that not all complex systems could be modelled as a hierarchy. Therefore non-hierarchic formulations were developed by Sobieszczanski-Sobieski[9] that relied on linearisation techniques via calculation of the global sensitivity equations[10]. Various other methods were developed from the initial multi-level optimisation frameworks. For example so-called ‘variable-complexity’ multi-disciplinary optimisation methods for the design of high-speed civil transport wings were originally proposed in Ref. 11 and extended with exploitation of response surface approximations for the computationally expensive detailed model evaluations[12].

Alternative techniques were proposed in Refs 13, 14 and 15, amongst others. These alternative techniques focussed on additional terms in the linearised coupling equations, construction of response surfaces to replace the global sensitivity equations and relaxation of the coupling via augmented Lagrangian relaxation. More recently, Paiva and co-workers[16] investigated the computational performance benefits in using these approximations in conjunction with multi-disciplinary design optimisation for the preliminary design of aircraft wings. They concluded that standard polynomial interpolation is only well-suited to very simple problems. At higher dimensionality, the usage of more complex kriging models and artificial neural networks can result in considerable performance benefits.

https://doi.org/10.1017/S0001924000008915 Published online by Cambridge University Press

Aircraft level optimisation of fuselage structures considers global level analyses of the fuselage structure while focusing on the sizing of local structural design variables that represent the thin-wall properties of the structure, like skin thicknesses and stringer dimensions[2]. The global analyses typically use (coarse) finite element (FE) models (e.g. of 10 or 20 fuselage frame bays) and consider basic sizing variables like skin thicknesses and stiffener cross section areas and account for global stress re-distribution during the global optimisation iterations. The local analyses typically use dedicated skill tools for very efficient evaluation of many different design criteria (buckling, reparability, damage tolerance, etc.) for local structural elements (e.g. so-called super-stringers[2] and consider detailed local sizing variables like composite laminate properties and detailed stiffener dimensions in the local optimisations. These skill tools are often developed in-house in industry and are based on simplified geometries and physical assumptions and equations. Hence there are some limitations of these dedicated skill tools, such as their limited validity for the specific conditions (geometry, loading, materials, etc) for which they were developed and the cost of maintenance and further development (related to legacy codes, programming choices) and validation of these tools[17]. Instead, more generic analysis tools like commercial FE codes can be used for the local analyses and optimisations (e.g. Refs 18 and 19), but because of the typical high computational cost of FE analysis this requires highly efficient evaluation procedures for these detailed local FE models.

This paper presents an innovative design method where detailed local FE analysis of panel buckling is applied in the global level optimisation. The required computational efficiency is achieved by advanced use of surrogate modelling methods[17,20], on the different levels, and by efficient representation of the optimised local configuration. This yields flexibility in the optimisation procedure and allows for efficient gradient based search methods as well as more costly GA-based search optimisations. In accordance with recommendations given in Refs 21 and 16 the more advanced methods like kriging models and artificial neural networks in combination with adaptive sampling algorithms are considered here for surrogate modelling.

Other investigations into exploiting efficient surrogate modelling approaches for representation of composite panel buckling behaviour were recently published, e.g. Refs 17 and 22, where simplified panel buckling analyses based on composite lamination parameters were considered. The method in the present paper makes direct use of FE panel buckling analyses, which can contain extensive detail. The method is applicable to composite structures but not specifically dedicated to these materials and will be demonstrated on a composite fuselage design case considering common structural sizing variables like thicknesses and stringer dimensions.

2.0 DESIGN PROBLEM

The design problem considered in this study is the weight optimisation of a realistic fuselage barrel structure representative of a forward section (located between the nose fuselage and the centre section) of a single aisle aircraft (Fig. 1). A number of realistic barrel sizing load cases is applied, including loads due to turbulence, manoeuvre, braking, taxiing, etc.

The considered cylindrical barrel is implemented as a 3D FE model (in this case in NASTRAN[22]) consisting of linear elements for all the relevant structural components like skins, frames, stringers, window frames, door surround structures, passenger floor and cargo floor structures. In this global finite element model (GFEM) of the barrel, typically each skin panel between two stringer and frame segments is represented with one linear shell element, each stringer segment and frame segment are represented with one linear rod and one linear beam element, respectively. The total barrel model comprises 21 frames with frame pitch of about 584mm and a total length of 11,786mm

https://doi.org/10.1017/S0001924000008915 Published online by Cambridge University Press

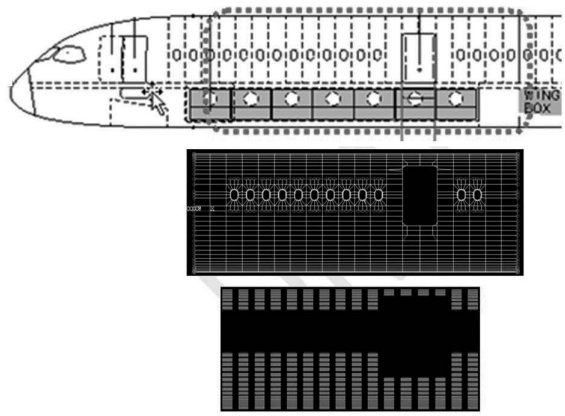


Figure 1. Side-view illustration of the location of the considered GFEM barrel model (middle) in the aircraft fuselage (upper) and indication of the global optimisation design regions as considered in the barrel model (lower: skin thicknesses in blue shell elements; stringer areas in red rod elements).

and has about 19k degrees of freedom (DOF). The barrel cross-section is (approximately) circular with mean radius of about 2,100mm. About 70 stringers are distributed over de circumference of the barrel with various stringer pitches (approximately 225, 210, 205, 185 and 170mm). Windows and doors are surrounded by specific stiffening structures consisting of rods, beams and thicker skins. Passenger and cargo floor structures are modelled by beams.

The fuselage barrel design problem is considered as the global level optimisation problem and is formulated as weight minimisation subject to a set of failure constraints:

$$\min_{x_g} M_g(x_g) \quad \ldots (1)$$

subject to

$$c_g(\Phi_g(x_g)) \leq 0. \quad \ldots (2)$$

Here M_g is the total mass of the barrel and x_g are the design variables on global level. The global level constraints c_g are based on strain criteria in skins and stringers which depend on the internal forces Φ_g that follow from the global level equilibrium for all considered load cases. The internal forces Φ_g depend on the global level variables x_g. The strain criteria used here are the following:

$$-0{\cdot}003 < \varepsilon_{skin} < 0{\cdot}005 \quad \ldots (3)$$

$$-0{\cdot}002 < \varepsilon_{stringer} < 0{\cdot}005 \quad \ldots (4)$$

The global design variables (x_g) in the present study are the skin thickness (defined for each shell element; bounds: $1{\cdot}6\text{mm} \leq x_{g\text{-}skin} \leq 8{\cdot}0\text{mm}$) and stringer cross sectional area (defined for each rod element; bounds: $101\text{mm}^2 \leq x_{g\text{-}stringer} \leq 457\text{mm}^2$). The global design variables as well as the global constraints are applied only in certain design regions of the barrel model, see Fig. 1 above. All other dimensions in the barrel model (i.e. all frames and all windows and doors surrounding areas and all floor structures) are unchanged.

https://doi.org/10.1017/S0001924000008915 Published online by Cambridge University Press

The GFEM barrel model is adequate for global structural analyses and the global level optimisation problem can be very efficiently solved for linear static analyses (in the present study by using the NASTRAN finite element method (FEM) solvers SOL101 for the linear static solution and SOL200 for the structural optimisation[22]). However, besides the basic strain criteria used here the optimisation should also take into account other (probably more critical) failure criteria, in particular related to buckling. But that would require other types of analyses and a (much) higher degree of detail in the structural modelling. For example, the local lay-up definitions of composite skins and stringers and detailed stringer dimensions (height, width, etc.) have strong influence on the local buckling behaviour. Therefore more detailed local level structural models (e.g. by dedicated so-called 'skill tools') are commonly used to analyse and optimise the local structures[2]. In this paper a local level detailed finite element model (DFEM) is applied to incorporate the local structural details and to take into account the local buckling behaviour. This DFEM model is further described in the following sections.

The aim on the barrel level is to incorporate the optimised local structure in an efficient and proper way in the global level optimisation. Therefore we stick to the efficient global level optimisation procedure described above and incorporate the optimised local structure via extra global-local constraints

$$c_{gl}(x_g, x_l^*(\Phi_g)) \leq 0 \quad \ldots (5)$$

These global-local constraints c_{gl} represent the coupling of the global level to the local level optimisation. Here x_l^* represent the optimised local variables, which are expressed as a function of the internal forces Φ_g. The global-local constraints here are simply formulated as

$$x_g \geq \xi_{gl}(x_l^*(\Phi_g)) \quad \ldots (6)$$

where ξ_{gl} represents the relation between the global and local level variables, which is typically a relatively simple analytical function (e.g. the relation between stringer cross sectional area and stringer variables like stringer height and cap width). These optimised local variables x_l^* result from the local level optimisation, which is expressed as

$$x_l^* = argmin(x_l)\, M_l(x_l) \quad \ldots (7)$$

subject to

$$c_l(x_l, \Phi_l) \leq 0 \quad \ldots (8)$$

Here M_l is the local specific mass (e.g. per unit of panel surface area) and x_l are the design variables on local level. c_l are the local level constraints, which are expressed in the local level variables and the local loading Φ_l which shall be consistent with the global internal forces Φ_g. The local level constraints represent the failure criteria related to local buckling.

3.0 PANEL MODEL

On the local level we use a DFEM model of a fuselage panel with loading, boundary conditions, and skin, stringer and frame details that are consistent with the GFEM barrel model. Critical loads for different failure modes can be calculated with this model, but the present study is limited to

https://doi.org/10.1017/S0001924000008915 Published online by Cambridge University Press

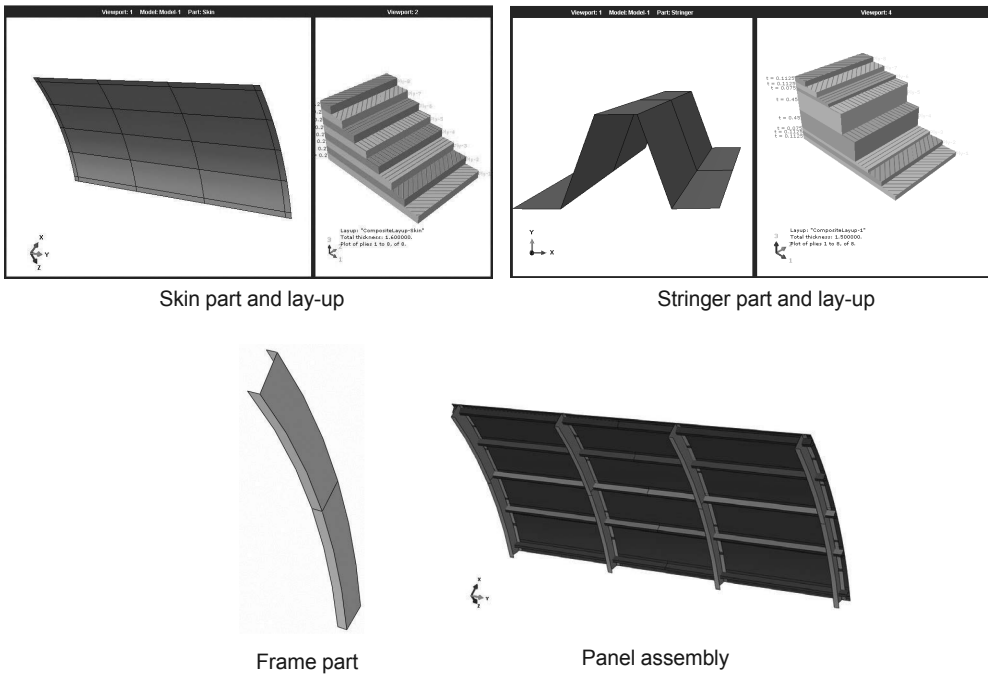


Figure 2. The DFEM panel model assembly and its parts. For skin and stringer the part geometries and the composite layups are shown. Frames are aluminium.

only buckling failure modes. The DFEM model is set up such that it allows for buckling load evaluation for any given local loading condition, which corresponds to the internal loading in the barrel. The detailed structural design variables are included as parameters in the DFEM model and thus can be optimised subject to constraints for the considered failure modes. For flexibility and ease of use, the local level optimisation is implemented as a surrogate based optimisation procedure. Therefore the DFEM model is evaluated for given sets of loadings and design variables combinations and the responses are collected and further processed into accurate surrogate models.

The detailed design of the panel structure in this study is based on composite skin, co-bonded composite omega stringers and aluminium C-frames. Mouseholes in the frames have been ignored. The frames and stringers are attached to the skin over the whole contact area by tie constraints. Fasteners could be used for stringer and frame attachment but have not been modelled in this study. The detailed panel model is built up from the three parts skin, stringer and frame, see Fig. 2, and is implemented in ABAQUS FEM software[24]. Five stringers and four frames are used in the panel assembly in order to obtain two central bays in the panel that have reasonable distance from the boundary conditions applied to the panel edges.

All the parts are modelled by quadratic shell elements. The Alu frames are modelled with isotropic linear elastic material (coefficients given below in Table 1). The skin and stringers are modelled as composite laminates with symmetric layups (45°/–45°/90°/0°)s where 0° is in the stringer-length direction. The ply thicknesses are tuned to match the total laminate thickness of skin and stringer, which are design variables in the local level optimisation. For the skin, equal ply thickness of 12·5% of total skin thickness for all plies is used. For the stringers variable ply thickness of (15%, 15%, 10%, 60%)s is used for each ply in the (45°/–45°/90°/0°)s lay-up. The

https://doi.org/10.1017/S0001924000008915 Published online by Cambridge University Press

Table 1
Material properties for composite plies of skin and stringers and for (isotropic) frame and local level design variables in DFEM panel model.

Material Property	Values for skin & stringer	Values for frame	Design variable	Lower/upper bounds
Ex	157 GPa	72 GPa	Sk. thickness:	$1{\cdot}6\text{mm} \leq t_{sk} \leq 2{\cdot}8\text{mm}$
Ey	8·5 GPa	72 GPa	Str. thickness:	$1{\cdot}5\text{mm} \leq t_{st} \leq 3{\cdot}0\text{mm}$
Gxy	4·2 GPa	–	Str. height:	$15\text{mm} \leq h_{st} \leq 30\text{mm}$
vxy	0·35	0·3	Str. cap width:	$15\text{mm} \leq w_{st} \leq 30\text{mm}$

considered materials are characterised by the coefficients in Table 1. The composite material is the same for skin and stringers. The DFEM panel model allows for consideration of many different design variables, like detailed structural sizing variables, stringer or frame pitches, material properties, composite lay-ups, stringer cap thickness, etc. To demonstrate the feasibility of the proposed approach, we limit this study to the set of local level design variables given in Table 1. The upper bounds of these variables are also limited because buckling is expected to be not a critical failure mode for higher values.

This choice of these local level design variables is related to the aims, the modelling and the variables that are used in the global level optimisation. In the present study the variables that are considered in the GFEM barrel optimisation are the skin thicknesses and stringer dimensions while stringer and frame pitches, frame dimensions and curvature radii remain constant. In accordance with the GFEM barrel model, a skin curvature radius of 2,100mm and frame pitch of 584mm are used. However, because the stringer pitch is not the same in all design regions in the GFEM model, but varies between about 170mm and 225mm, this stringer pitch variation shall also be accounted for in the DFEM panel optimisations.

The boundary conditions in the DFEM panel model should resemble the edge conditions as would be experienced by the panel in the global GFEM model under the given load. This is simplified to the following cylindrical boundary conditions for the panel:

- All three rotations of all skin edges (straight and curved edges) are suppressed;
- All radial displacements of all skin edges (straight and curved edges) are suppressed;
- All tangential displacements of the straight skin edges are constrained by a linear interpolation between their end nodes such that their angular rotation about the fuselage axis is linear over the full length of these edges;
- All three rotations of all frames and stringer end-cross-sections (i.e. near the straight and curved edges of the panel) are suppressed;
- Tangential and axial displacements of one skin corner point are suppressed to avoid rigid body motion.

In the local level analyses the loading in the DFEM panel model shall be representative for the internal loads in the global level GFEM model. To account for all the relevant internal loadings occurring in the GFEM model, the panel loading is defined as axial compression/tension, shear and tangential compression/tension. The loads are applied as uniform edge loads (i.e. load intensities expressed in N/mm) on the skin at the panel edges: tension/compression at the curved edges (Nx),

https://doi.org/10.1017/S0001924000008915 Published online by Cambridge University Press

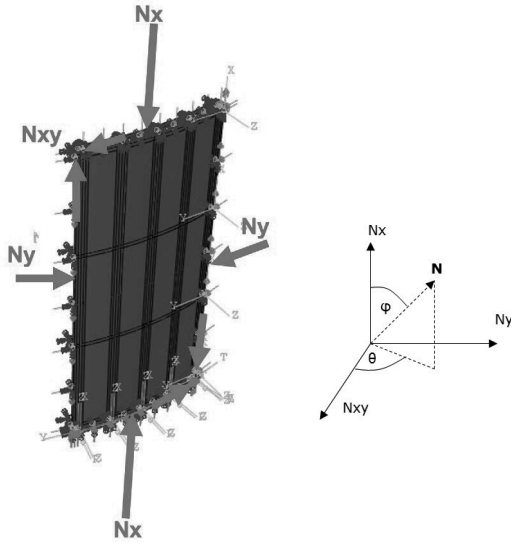


Figure 3. Illustration of the loading in the panel model; edge loads (in *N*/mm) in the DFEM panel model (left) and definition of the 3D load vector **N** in spherical co-ordinates (right).

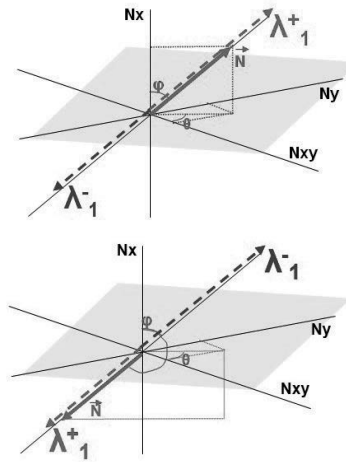


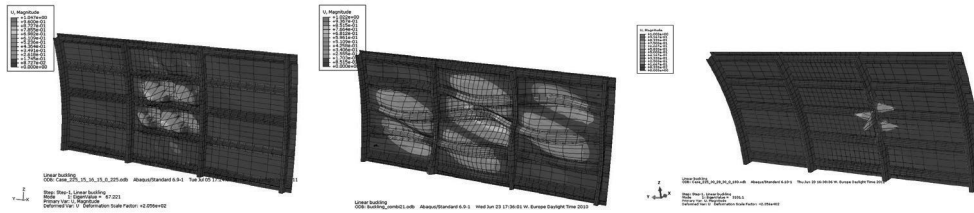
Figure 4. Illustration of the 3D load vector **N** for which the first positive and first negative buckling eigenvalues are shown (left); for the opposite loading (right), in general, exactly the opposite values for the first positive and first negative buckling eigenvalues are found.

tension/compression at straight edges (*Ny*), shear at curved and straight edges (*Nxy*). The resulting load vector is represented as a 3D load vector **N** = (*Nxy*, *Ny*, *Nx*). This load vector is expressed in the spherical co-ordinates (θ, φ, *r*), where $|\mathbf{N}| = r$, $Nx = r\text{Cos}(\varphi)$, $Ny = r\text{Sin}(\varphi)\text{Sin}(\theta)$ and $Nxy = r\text{Sin}(\varphi)\text{Cos}(\theta)$.

Because we use linear analysis at the local level, we only consider the unit load $|\mathbf{N}| = 1$. Therefore the loading in the DFEM panel model can then be fully parametrically defined by the angular co-ordinates (θ, φ). The considered ranges for the spherical angular co-ordinates (θ, φ) are $\theta \in [0,2\pi\rangle$, $\varphi \in [0, \pi\rangle$. Note that the cases $\theta = 2\pi$ and $\varphi = \pi$ have been excluded in these ranges because $\mathbf{N}(\theta = 0,\varphi) = \mathbf{N}(\theta = 2\pi, \varphi)\forall\varphi$ and because $\mathbf{N}(\theta,\varphi = \pi)\forall\theta$ represents the axial tension loading, which would not yield sensible DFEM buckling analysis results and would deteriorate the reliability of the local level surrogate models. It should be noted that the buckling eigenvalues are evaluated for each unit load combination (*Nxy*, *Ny*, *Nx*). Each of these load components can be positive, yielding compression for (*Ny*, *Nx*) (in accordance with the definition of edge loads in ABAQUS[24]), or negative, yielding tension for (*Ny*, *Nx*). Hence for each load combination, there exists another load combination that is exactly the opposite; see Fig. 4. From a symmetry point of view, only the load combinations with at least one compression component would need to be evaluated. However, in general it cannot obviously be pre-determined whether a load combination yields a compression-dominated (i.e. first eigenvalue is positive) or tension-dominated (i.e. first eigenvalue is negative) buckling response. Therefore each possible load combination is evaluated and only the first positive buckling eigenvalues (λ_1^+) are computed.

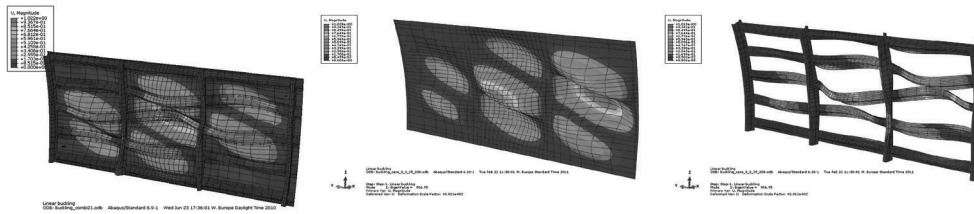
Moreover, the apparent geometric symmetry of the panel seems to imply equal buckling values for load cases with opposite shear loadings (±*Nxy*, *Ny*, *Nx*). However, this shear-symmetry is not the case due to the directional dependency of (mainly) the skin bending stiffness for shear loading. In other words: because the outer skin plies have 45° angles, there is 'directional preference' for the shear loading that is applied and the skin modes that occur. The linear buckling analyses with the

https://doi.org/10.1017/S0001924000008915 Published online by Cambridge University Press



Skin buckling mode | Global buckling mode | Frame buckling mode

Figure 5. Illustration of various possible buckling mode shapes found with the DFEM panel model.



Global buckling mode | Skin displacements | Stringer-frame displacements

Figure 6. Illustration of separate displacement fields of skin, stringers and frames in a global buckling mode of the DFEM panel model.

DFEM model are intended to efficiently capture the relevant panel buckling behaviour. Because of the detail in the geometry and mesh of the DFEM model, different buckling mode-shapes will arise depending on the applied loading and on the detailed design variables. Besides local skin buckling modes, also global modes and frame modes may occur. See Fig. 5.

To distinguish between the various buckling mode types, the deformation fields of the mode shapes are evaluated and the maximum displacements of skin, stringers and frames are separately retrieved.

The type of mode is determined according to the following criteria:

1. Skin mode: $\max(u_{skin}) > f_{mode} \max((u_{stringer}),(u_{frame}))$
2. Frame mode: $\max((u_{frame}), (u_{stringer})) > f_{mode} \max(u_{skin})$
3. Global mode: in all other cases.

where $u_{skin} = \{|u^1_{skin}|,\ldots,|u^{nskin}_{skin}|\}$, $u_{stringer} = \{|u^1_{stringer}|,\ldots,|u^{nstringer}_{stringer}|\}$, $u_{frame} = \{|u^1_{frame}|,\ldots,|u^{nframe}_{frame}|\}$

are the arrays with the absolute displacement values in all the ($_{nskin,\ nstringer,\ nframe}$) nodes of the skin, stringers and frames, respectively, in the DFEM model. The variable f_{mode} is a mode factor to distinguish between skin- and frame or stringer modes, for which a value of 10·0 was used here. Note that the frame modes include the modes where maximum displacement occurs in stringers. The accuracy or reliability of the global and frame buckling modes will be less than for the skin modes because the DFEM panel model is less adequate for prediction of these types of buckling. But it should be noted that these global and frame buckling modes will mostly occur for relatively high skin thickness values (e.g. > 2·2mm) for which the buckling constraint will be less critical in the global level optimisation.

https://doi.org/10.1017/S0001924000008915 Published online by Cambridge University Press

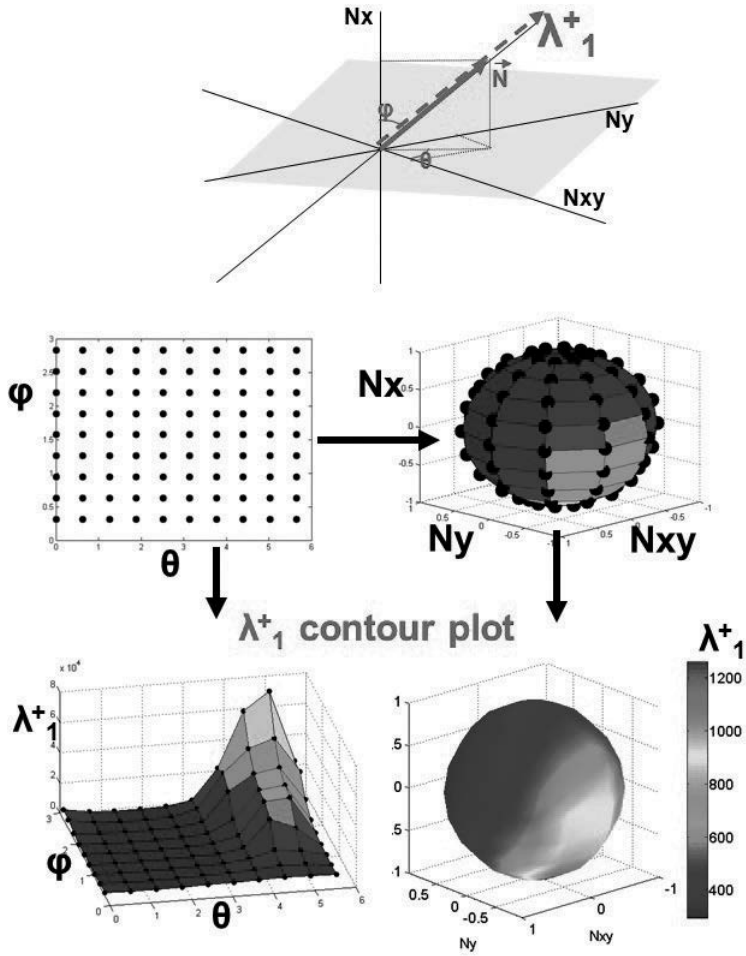


Figure 7. Illustration of the load sampling and resulting buckling values for just one combination of the local design variables t_{sk}, t_{st}, h_{st}, w_{st}.

The DFEM panel model contains in total about 3·5k quadratic shell elements (ABAQUS element code S8R: eight-node doubly curved thick shell, reduced integration[24]), yielding about 11k nodes and about 40k DOF. The DFEM panel model is deployed in linear buckling analyses that are executed for any given loading condition and local design variable combination. These analyses are run in ABAQUS Standard 6·11[24] using the Lanczos solver. The first 10 positive eigenvalues and corresponding buckling mode shapes are retrieved. This analysis requires about 100s on a standard PC (Intel Core2 Duo, 2·93 GHz, 3GB RAM), or about 30s on a compute server (SGI Altix ICE8200, Intel Xeon Quad Core, 2·6 GHz, 24GB RAM, 8 CPU/node). From these 10 mode shapes, ordered by increasing buckling eigenvalue, it was determined which were the first skin mode, global mode and frame mode to occur. Then the lowest eigenvalues for skin buckling (λ_{sk}), global buckling (λ_{gl}) and frame buckling (λ_{fr}) were retrieved and stored for each given loading condition and local design variable combination.

https://doi.org/10.1017/S0001924000008915 Published online by Cambridge University Press

4.0 PANEL POST-BUCKLING VERIFICATIONS

For computational efficiency the panel buckling loads are computed by linear buckling analysis (ABAQUS Lanczos solver[24]; ~30s CPU time on single node of compute server). As a small verification of the linear buckling load predictions, the skin, global and frame buckling values for some load cases were checked with non-linear post-buckling analysis (ABAQUS Riks solver[24]; ~2,000s CPU time on single node of compute server). The linear mode shapes and buckling values were reasonably reproduced by the non-linear analyses, but only few load cases were checked. Panel optimisation fully based on non-linear buckling analyses would be obviously much more complex and expensive and was therefore not further considered in this study.

5.0 PANEL SURROGATE MODELS

For the creation of the surrogate models of the DFEM panel model buckling behaviour, large series of analysis runs are executed to sample different combinations of all the variables in the DFEM panel model: the spherical angular co-ordinates (θ, φ) for the load combinations, and the local design variables (t_{sk}, t_{st}, h_{st}, w_{st}). (Note: the dependency on the stringer pitch variation is handled later in the process.) A traditional design of experiment (DOE) based on full-factorial sampling with ($11 \times 7 \times 5 \times 4 \times 4 \times 4 = 24{,}640$) design points for the six variables (θ, φ, t_{sk}, t_{st}, h_{st}, w_{st}) was used here. Recall that the loads for $\theta = 0, \forall\varphi$ are exactly the same as for $\theta = 2\pi, \forall\varphi$ and therefore need only be evaluated for $\theta = 0, \forall\varphi$, and the single evaluation of pure axial compression loading ($\varphi = 0, \theta = 0$) can be assigned to all $\varphi = 0, \forall\theta$. See Fig. 7 as an illustration of the (θ, φ) sampling of the first positive buckling eigenvalues (λ_1^+).

Although this type of DOE normally requires more data points than for example latin-hypercube sampling (LHS), it has some advantages in the ease of application and certain assessments on sub sets of the data that are done later in the procedure. In each of the design points the first 10 buckling eigenvalues and their corresponding mode-shapes were evaluated from which the skin/stringer/frame maximum displacement values were derived. Then each of these 10 buckling eigenvalues are checked against the buckling mode type criteria given above and the lowest values found for the skin, global and frame buckling loads (λ_{sk}, λ_{gl}, λ_{fr}) are stored for each design point, yielding (λ_{sk}, λ_{gl}, λ_{fr}) as a function of the DOE variables (θ, φ, t_{sk}, t_{st}, h_{st}, w_{st}). Note that at least one, but not necessarily all three, of the (λ_{sk}, λ_{gl}, λ_{fr}) is found in each design point. From the resulting large data sets, six-dimensional surrogate models of the DFEM panel buckling load values are created (skin buckling: $\tilde{\lambda}_{sk}(\theta, \varphi, t_{sk}, t_{st}, h_{st}, w_{st})$; global buckling: $\tilde{\lambda}_{gl}(\theta, \varphi, t_{sk}, t_{st}, h_{st}, w_{st})$; frame buckling: $\tilde{\lambda}_{fr}(\theta, \varphi, t_{sk}, t_{st}, h_{st}, w_{st})$).

A number of different surrogate modelling methods are considered, including standard least-squares regression with various polynomial orders (e.g. full first, second and third order polynomials, indicated here by the codes poly_1, poly_2, poly_3, respectively), generalised regressions (indicated here by the code poly_glm, etc.), artificial neural nets (ANNs), radial basis functions (RBFs), mixture of experts (MoEs) (for further information see Refs 20, 25). The surrogate modelling and quality assessment is performed in an efficient way using the MultiFit[20] software tool, which is developed in Matlab[25]. For example, the quality metrics evaluated for various surrogate models created for the skin buckling value ($\tilde{\lambda}_{sk}(\theta, \varphi, t_{sk}, t_{st}, h_{st}, w_{st})$) yields the following results in the Table 2.

Obviously, the feed-forward ANN with two hidden layers with respectively 50 and 10 nodes (coded here as ann-5010 model) yields the best accuracy for these data. In fact, also for the frame and global buckling data (λ_{fr} and λ_{gl}) the ann-5010 surrogate model provided appropriate accuracy.

https://doi.org/10.1017/S0001924000008915 Published online by Cambridge University Press

Table 2
Different surrogate models (poly_1, etc) and the values for their quality metrics (coded here as mape, maxape, etc., see first two columns in the table) evaluated for the skin buckling value data ($\tilde{}_{sk}$)

		poly_1	poly_2	poly_3	poly_glm	poly_pls	poly_regress	poly_robust	poly_step	ann-20	ann-5010
mape	mean absolute percentage error	54,12	40,64	37,40	37,40	37,40	37,40	17,48	101,16	8,44	2,01
maxape	max absolute percentage error	316,05	331,81	203,07	203,07	203,07	203,07	89,38	498,97	77,92	25,19
10%quant	10% error quantile	17,72	24,48	17,67	17,67	17,67	17,67	42,79	7,48	71,15	98,90
5%quant	5% error quantile	8,71	12,52	8,75	8,75	8,75	8,75	21,15	3,63	45,24	91,21
mse	mean square error	45435,62	34828,15	25942,91	25942,91	25942,91	25942,91	44240,92	66596,99	884,09	57,54
rmse	root mean square error	213,16	186,62	161,07	161,07	161,07	161,07	210,34	258,06	29,73	7,59
rsquare	coefficient of determination	0,27	0,44	0,58	0,58	0,58	0,58	0,29	-0,08	0,99	1,00
raae	relative average absolute error	0,50	0,40	0,37	0,37	0,37	0,37	0,30	0,81	0,08	0,02
aae	average absolute error	123,28	100,54	92,70	92,70	92,70	92,70	75,46	202,08	18,81	4,68
rmae	relative maximum absolute error	10,45	9,82	9,06	9,06	9,06	9,06	11,07	7,69	2,72	0,59
mae	mean absolute error	2601,28	2443,73	2254,46	2254,46	2254,46	2254,46	2754,68	1913,61	678,02	146,40

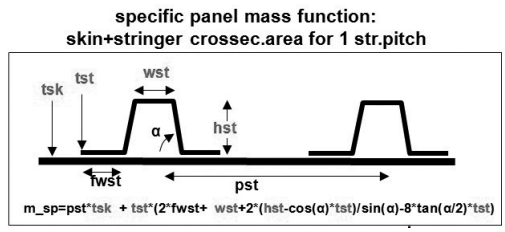


Figure 8. Illustration of the panel model specific cross-sectional area calculation.

6.0 PANEL LEVEL OPTIMISATIONS

Once the surrogate models of the DFEM panel buckling values are available, the optimisations of the panel can be done very efficiently, exploiting various optimisation algorithms (gradient based, SQP (sequential quadratic programming), GAs, etc.) and if desired the analytical derivatives of objective and constraints may be exploited. The objective that is considered in the panel optimisations is the specific panel mass (m_{sp}, expressed here as cross-sectional area because the mass density of skin and stringers are equal), which is defined as function of the local design variables (t_{sk}, t_{st}, h_{st}, w_{st}) for a fixed stringer pitch (p_{st}), see Fig. 8.

The constraint functions in these optimisations are based on the buckling policy that is applied for the panel model according to the following criteria:

- no skin buckling shall occur below 0·7 limit-load (*LL*) for axial compression and 1·0 *LL* for shear (i.e.: $Nxy = 0{\cdot}0$: $LL_{crit} = 0{\cdot}7$LL; $Nx = 0{\cdot}0$: $LL_{crit} = 1{\cdot}0LL$);
- an interpolated criterion between 0·7 and 1·0 is applied for combined compression-shear loading (i.e.: $Nxy \neq 0{\cdot}0 \wedge Nx \neq 0{\cdot}0$: $LL_{crit} = LL(0{\cdot}7 + 0{\cdot}3\ \text{Arctan}(|Nxy/Nx|))/(\pi/2)$;
- no global or frame buckling shall occur below ultimate load (*UL*).

The load cases that are applied in the barrel level GFEM model represent ultimate loads. Hence the load level ($F = |\mathbf{N}|$) applied in the DFEM, which corresponds to the internal load level in the GFEM model, is also considered as *UL* (i.e. $F = UL$). Limit load is defined as: $LL = UL/1{\cdot}5$. The above mentioned buckling criteria are therefore accordingly incorporated in the panel level

https://doi.org/10.1017/S0001924000008915 Published online by Cambridge University Press

optimisation formulation as follows:

Given (θ, φ, *F*)

$$\min_{t_{sk}, t_{st}, h_{st}, w_{st}} m_{sp}(t_{sk}, t_{st}, h_{st}, w_{st}) \quad \ldots (9)$$

subject to

$$\tilde{\lambda}_{sk}(\theta, \varphi, t_{sk}, t_{st}, h_{st}, w_{st}) > LL_{crit}(\theta, \varphi, F) \quad \ldots (10)$$

$$\tilde{\lambda}_{gl}(\theta, \varphi, t_{sk}, t_{st}, h_{st}, w_{st}) > UL(F) \quad \ldots (11)$$

$$\tilde{\lambda}_{fr}(\theta, \varphi, t_{sk}, t_{st}, h_{st}, w_{st}) > UL(F) \quad \ldots (12)$$

where the objective function m_{sp} is the analytical expression given above and the constraint functions are given by the surrogate models of the panel buckling loads ($\tilde{\lambda}_{sk}$, $\tilde{\lambda}_{gl}$, $\tilde{\lambda}_{fr}$). These panel level optimisations are performed for series of load combinations (θ, φ, *F*), where θ ∈ [0,2π>, φ ∈,[0,2π> and a range for *F* [F_{min}, F_{max}] is determined as follows: Because the objective m_{sp} is monotonically increasing in each of its variables (t_{sk}, t_{st}, h_{st}, w_{st}), the minimum m_{sp} is determined by the lower bounds of the variables ((t_{sk}, t_{st}, h_{st}, w_{st})$_{min}$) if none of the buckling constraints are active. This is the case for low values of *F*, such that LL_{crit} and *UL* are lower than the minimum buckling values occurring in each load combination (θ, φ). Therefore an approximate minimum value for *F* below which the buckling constraints are in-active is determined from the buckling data values:

$$F_{min}(\theta, \varphi) = min((1 \cdot 5 \frac{LL}{LL_{crit}} \lambda_{sk}(\theta, \varphi)), \lambda_{gl}(\theta, \varphi), \lambda_{fr}(\theta, \varphi)) \; \forall \; (t_{sk}, t_{st}, h_{st}, w_{st}) \quad \ldots (13)$$

Similarly an approximate maximum value for *F* is determined, above which the optimisations are infeasible because all three constraints cannot be fulfilled:

$$F_{max}(\theta, \varphi) = max((1 \cdot 5 \frac{LL}{LL_{crit}} \lambda_{sk}(\theta, \varphi)), \lambda_{gl}(\theta, \varphi), \lambda_{fr}(\theta, \varphi)) \; \forall \; (t_{sk}, t_{st}, h_{st}, w_{st}) \quad \ldots (14)$$

Note that the full-factorial sampling scheme that was applied has the advantage here that all the data samples for (λ_{sk}(θ,φ), λ_{gl}(θ,φ), λ_{gr}(θ,φ)) are available for each sampled combination of (t_{sk}, t_{st}, h_{st}, w_{st}). Series of load combinations (θ,φ,*F*) are then defined for the above mentioned ranges. The same (θ,φ) sampling as in the previous full-factorial DOE is used. Because of the high variability over (θ,φ) of the range of the force (*F*), that is first transformed by a log (log(*F*)) for which then an equidistant sampling of 20 points is applied. This results in 'partial-factorial' sampling in (θ,φ,*F*) of about 1,200 points in each of which the above mentioned panel level optimisation problem is solved. Figure 9 shows the set of load points in which the DFEM optimisations are run and the resulting optimised panel level variables for one of these load points.

Various optimisation algorithms may be used (e.g. SQP, interior-point, active-set, or other algorithms like GAs or pattern search). In the present study it was found that the gradient algorithm with active-set (based on Matlab's fmincon function[25]) showed the best performance. These

https://doi.org/10.1017/S0001924000008915 Published online by Cambridge University Press

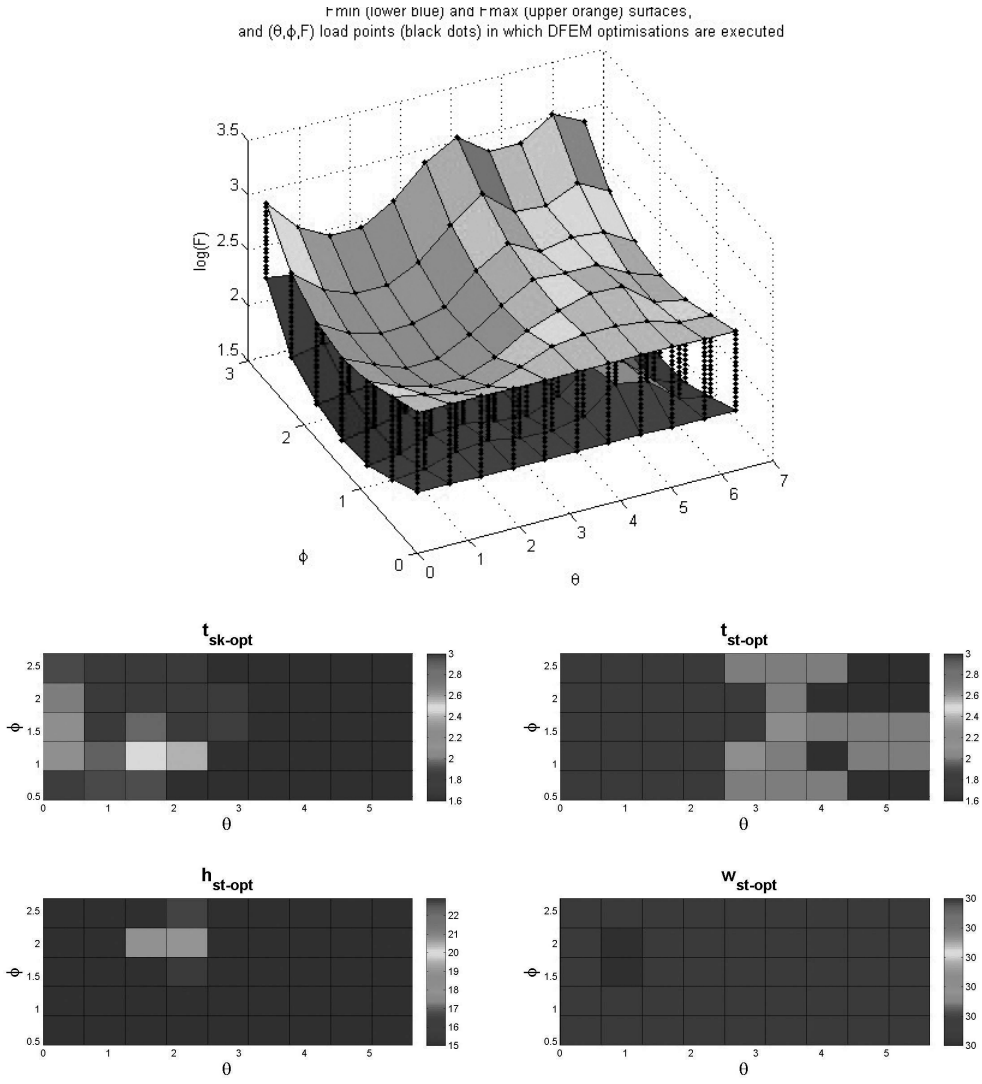


Figure 9. Illustration of the sampling in (θ,φ,*F*) of about 1,200 points in each of which the above mentioned panel level optimisation problem is solved (upper graph), and of the optimised panel level variables (t_{sk}, t_{st}, h_{st}, w_{st}) as a function of the load condition (θ, φ) for a fixed force value (*F*) (lower graphs).

optimisations can be run in parallel but because these optimisations are relatively simple and can be executed with about single-second compute time on standard PCs, sequential execution requires about 30 minutes which is quite acceptable. This sequential execution has the advantage that the optimum in one (θ, φ, *F*) point can be used as starting point for the optimisation in the next neighbouring (θ, φ, *F*) point. It should also be noted that alternative formulations of the local level optimisations can be easily implemented and evaluated, e.g. by minimising m_{sp} for series of given (θ, φ, *F*, t_{sk}) that would yield the optimum stringer dimensions $(t_{st}, h_{st}, w_{st})_{opt}$ as a function of loading and skin thickness (θ, φ, *F*, t_{sk}). The results of these optimisations yield the data set of optimised values of (t_{sk}, t_{st}, h_{st}, w_{st}) as function of (θ, φ, *F*).

https://doi.org/10.1017/S0001924000008915 Published online by Cambridge University Press

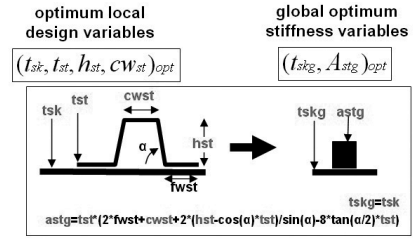


Figure 10. Illustration of the relation between the global and local level variables.

Table 3
Different surrogate models (coded as poly–1, etc.) and their quality metrics (coded as mape, etc.) values evaluated for the optimised global skin thickness data ($\tilde{t}_{skgopt}(\theta, \varphi, F)$

		poly_1	poly_2	poly_3	poly_glm	poly_pls	poly_regress	poly_robust	poly_step	ann-20	ann-4010
mape	mean absolute percentage error	14,81	10,56	8,13	8,13	8,13	8,13	8,01	28,72	2,89	1,05
maxape	max absolute percentage error	48,08	51,76	41,67	41,67	41,67	41,67	57,57	101,42	18,91	14,45
10%quant	10% error quantile	38,19	58,93	73,97	73,97	73,97	73,97	77,20	21,84	98,01	99,66
5%quant	5% error quantile	18,41	33,45	39,56	39,56	39,56	39,56	46,70	11,95	83,38	98,15
mse	mean square error	0,14	0,08	0,05	0,05	0,05	0,05	0,05	0,49	0,01	0,00
rmse	root mean square error	0,37	0,29	0,21	0,21	0,21	0,21	0,23	0,70	0,08	0,03
rsquare	coefficient of determination	0,26	0,56	0,76	0,76	0,76	0,76	0,71	-1,65	0,97	0,99
raae	relative average absolute error	0,71	0,51	0,38	0,38	0,38	0,38	0,37	1,32	0,14	0,05
aae	average absolute error	0,31	0,22	0,16	0,16	0,16	0,16	0,16	0,57	0,06	0,02
rmae	relative maximum absolute error	1,97	2,01	1,73	1,73	1,73	1,73	2,31	4,20	1,22	0,60
mae	mean absolute error	0,85	0,87	0,74	0,74	0,74	0,74	0,99	1,81	0,53	0,26

$$(t_{sk}, t_{st}, h_{st}, w_{st})_{opt} = f_{x-opt}(\theta, \varphi, F) \quad ; \quad F \in [F_{min}(\theta, \varphi), F_{max}(\theta, \varphi)] \qquad \ldots (15)$$

As described above, the optimised values of (t_{sk}, t_{st}, h_{st}, w_{st}) are equal to their minimum bounds in case the load value F is below the minimum.

$$(t_{sk}, t_{st}, h_{st}, w_{st})_{opt} = (t_{sk}, t_{st}, h_{st}, w_{st})_{min} \quad ; \quad F < F_{min}(\theta, \varphi) \qquad \ldots (16)$$

In order to evaluate if the load value F is below or above the minimum ($F < F_{min}(\theta, \varphi)$)) a surrogate model representation of $F_{min}(\theta, \varphi)$ is also required, which is achieved with quite good accuracy by a second order polynomial moving-least-squares fit[20].

The set (t_{st}, h_{st}, w_{st})$_{opt}$ represents, for a given load state expressed by (θ, φ, F), the optimised panel design in terms of the local design variables; see illustrations in Fig. 9 above. The data set of these optimised local variables is transformed to the optimised global stiffness variables (skin thickness and stringer cross sectional area) according to (see also Fig. 10):

$$t_{skgopt} = t_{skopt} \qquad \ldots (17)$$

$$A_{stgopt} = \xi_{gl}((t_{sk}, t_{st}, h_{st}, w_{st})_{opt}) \qquad \ldots (18)$$

The data sets of these two optimised global variables are then fit into surrogate models as function of the loading condition: Surrogate model of optimised global skin thickness: $\tilde{t}_{skgopt}(\theta, \varphi, F)$ and Surrogate model of optimised global stringer cross sectional area: $\tilde{A}_{skgopt}(\theta, \varphi, F)$.

Again, various methods including polynomial regression and ANN's were applied using the MultiFit[20] software tool (see Table 3), resulting finally in the best accuracy for the feed-forward ANN with two hidden layers with respectively 40 and 10 nodes (coded here as ann-4010).

https://doi.org/10.1017/S0001924000008915 Published online by Cambridge University Press

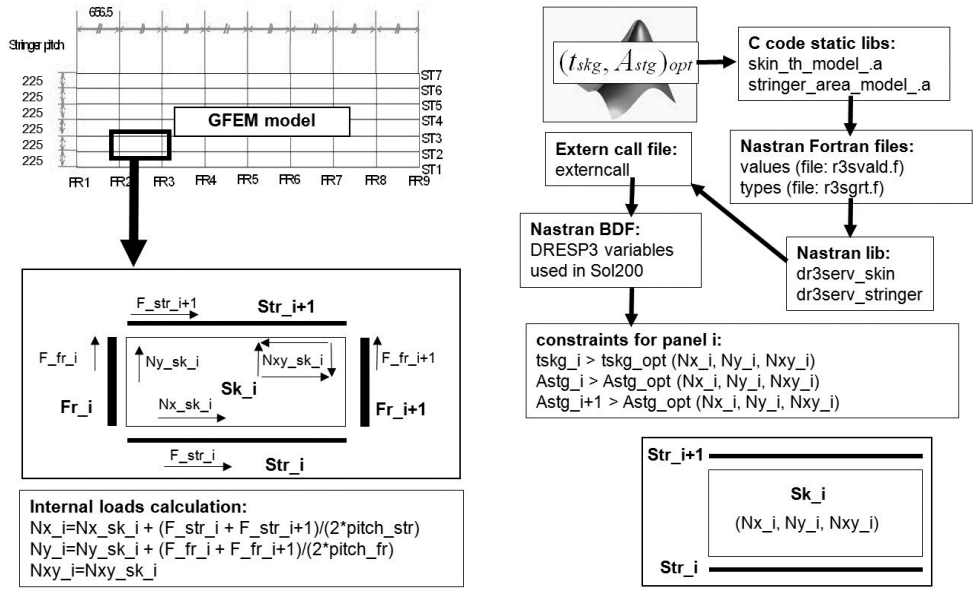


Figure 11. Left: illustration of the internal loads (*Nxy_i,Ny_i,Nx_i*) computation in a skin bay element (*Sk_i,*) with contributions from the neighbouring stringers (*Str_i, Str_i+1*) and frames (*Fr_i, Fr_i+1*), accounting for the actual stringer pitch (*pitch_str*) and frame pitch (*pitch_fr*);
Right: Illustration of the process to incorporate the Matlab surrogate models of the optimum global variables $(t_{skg}, A_{stg})_{opt}$ in the Nastran SOL200 optimisation, yielding the constraints for skin thickness of each skin element (*Sk_i*) and cross-sectional area of each stringer element (*Str_i, Str_i+1*).

It was found that these surrogate models were difficult to create with sufficient accuracy, especially for the stringer cross sectional area. This was due to the high gradients that were found in the optimum data set. However, the (local) accuracy of the surrogate models is expected to improve if actual load cases (expressed in (θ, φ, *F*)) coming from the global level are evaluated and optimised on the local level ('adaptive surrogate models').

As mentioned earlier, in the GFEM several different stringer pitch values occur (between about 170 and 225mm) that should be accounted for by the surrogate models predictions. This is achieved through straight-forward linear interpolation between the predictions of the optimised global variables surrogate models that were created according to the above described procedure for the smallest and largest stringer pitch values. As such the super-positions of the optimised global variables surrogate models can be defined that also include stringer pitch p_{st} as independent variable ($\tilde{t}^{p}_{skgopt}(\theta, \varphi, F, p_{st})$ and $(\tilde{A}^{p}_{skgopt}(\theta, \varphi, F, p_{st})$. Note that this linear interpolation for p_{st} has limited accuracy but can be easily improved by including more than two values for p_{st}, or by creating separate surrogate models ($\tilde{t}_{skgopt}(\theta, \varphi, F)$, $\tilde{A}_{skgopt}(\theta, \varphi, F)$). for each value of p_{st} that occurs in the GFEM.

https://doi.org/10.1017/S0001924000008915 Published online by Cambridge University Press

7.0 GLOBAL-LOCAL DATA INTERFACE

The surrogate models of the optimised global variables are then used in the barrel level optimisation that is executed by a NASTRAN SOL200 evaluation. In this evaluation the values of the optimised global variables are predicted by the surrogate models as a function of the internal loads in the barrel. The internal loads are determined in each skin bay in the design regions of the GFEM model from the (*Nxy*, *Ny*, *Nx*) load contributions from the skin, stringers and frames elements; see Fig. 11.

The SOL200 NASTRAN optimisation is achieved by encapsulation of the optimised global variables surrogate models (that are first created in Matlab and then ported to C-code libraries) in FORTRAN code libraries (function file r3svald.f) which are accessed by the D3RESP variables in the NASTRAN SOL200 run (see Fig. 11). The optimum values are assigned to the constraints for skin thickness of each skin element and cross-sectional area of each stringer element. Note that in the GFEM model the skins are modelled in NASTRAN by four-node shell elements (element code CQUAD4 with PSHELL properties[22]) with anisotropic membrane and bending stiffnesses (MAT2 material properties[22]). As the bending stiffness depends on the skin thickness (proportional to t^2_{skgopt}), these bending properties are also updated.

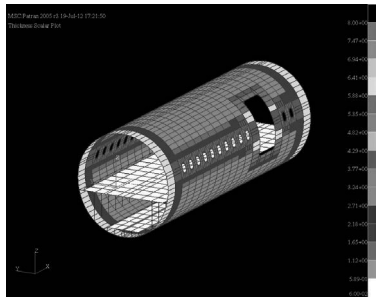
8.0 BARREL LEVEL OPTIMISATIONS

As mentioned above, the GFEM barrel model is implemented in NASTRAN and the global level optimisation problem is solved with SOL200[22] where the global objective is the total mass of the barrel structure (coded as a DRESP1 variable in NASTRAN). The global design variables are the skin thickness and stringer cross sectional area in the design regions of the barrel model, yielding a total number of 1,584 design variables (coded as DESVAR in NASTRAN), 792 for skin thickness and 792 for stringer area. The global level constraints are implemented as 1,584 constraint functions for skin strain and 792 constraint functions for stringer strain (coded as DCONSTR constraints and DRESP1 variables in NASTRAN), and 2280 constraint functions of external variables (coded as DCONSTR constraints and DRESP3 variables in NASTRAN) for the optimum skin thickness and stringer area. Hence, the global level optimisation comprises 4656 constraint functions that need to be evaluated for each of the 15 load cases, yielding 69,840 constraints in total. The initial values of the design variables are set to 3mm for skin thickness and 457mm^2 for stringer cross sectional area, yielding an initial total barrel mass of 1,676 kg. (Recall: the lower and upper bounds of the design variables are set to 1·6mm and 8·0mm for skin thickness and 101mm^2 and 457mm^2 for stringer cross sectional area.) The solution process of this optimisation problem requires about four hours on a standard workstation (Dual Quad-Core Intel Xeon, 2·3GHz, 16GB RAM). In the optimisation especially the memory usage and disk I/O and data storage (tens of GBs) are quite large, which is due to the large matrices in the optimisation resulting from the ~1·5k variables and ~70k constraints. The SOL200 solution requires eight major iterations to achieve the final optimum. The total mass of the optimum barrel design has decreased from 1,676kg to 1,226kg (about 25% improvement).

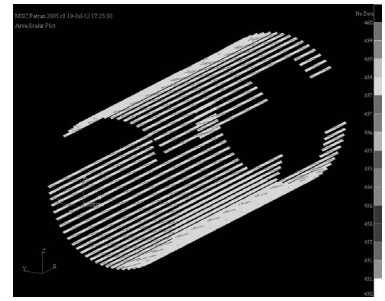
In the optimised barrel the skin thickness and stringer areas decreased to their lower bound in almost the complete design region, which are about 1·6mm and 101mm^2. Strains inside and outside design regions are within constraint values, i.e. the strain constraints are not active in the optimum design, and the strains outside the design regions have allowable levels.

The GFEM barrel optimisation yields the minimum design in almost the whole barrel. Consequently the optimum is driven by the lower bounds of the design variables (in almost the

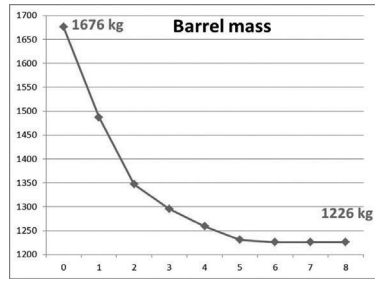
https://doi.org/10.1017/S0001924000008915 Published online by Cambridge University Press



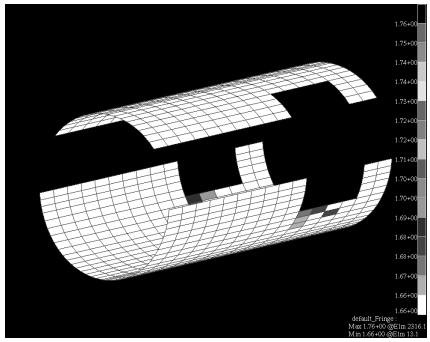
Initial skin thickness is 3mm



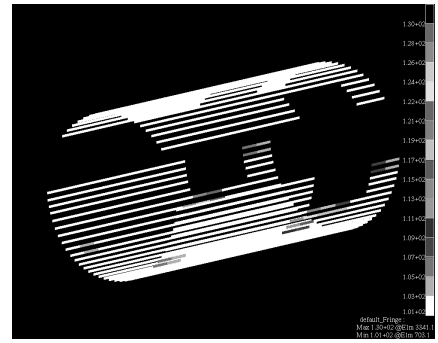
Initial stringer cross sectional area 457mm^2



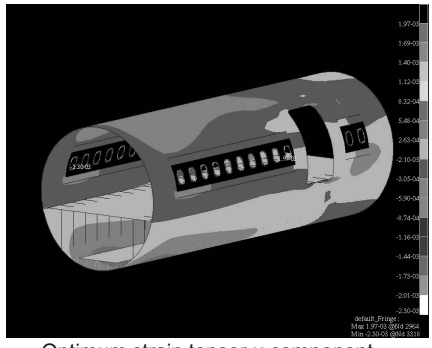
Total barrel mass during SOL200 iteration



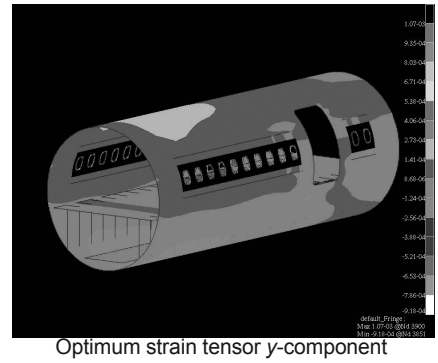
Optimum skin thickness



Optimum stringer cross sectional area



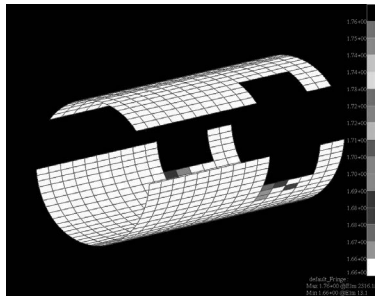
Optimum strain tensor *x*-component



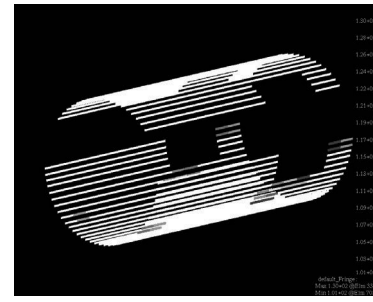
Optimum strain tensor *y*-component

Figure 12. Skin thickness distribution and stringer areas in the initial barrel configuration (upper row) and the barrel mass during the SOL200 iteration (middle row). For the optimised barrel (lower two rows) the skin thickness, stringer areas and strain tensor *x*-components and *y*-components are shown.

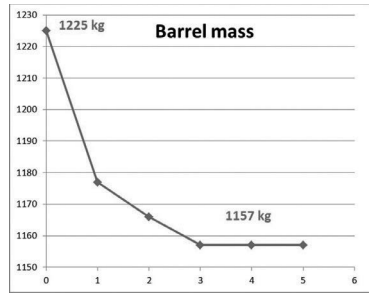
https://doi.org/10.1017/S0001924000008915 Published online by Cambridge University Press



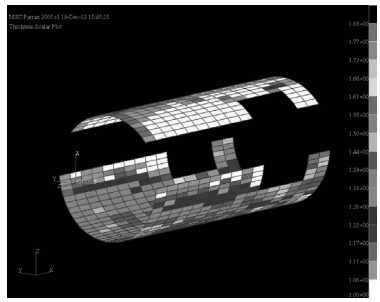
Initial skin thickness 1·6mm



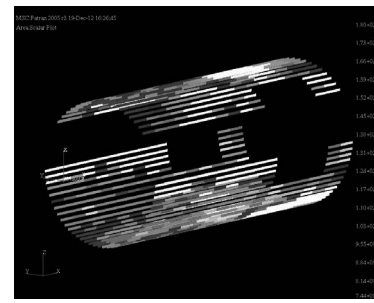
Initial stringer cross sectional area 101mm^2



Total barrel mass during SOL200 iteration



Optimum skin thickness



Optimum stringer cross sectional area

Figure 13. For the updated barrel optimisation, the skin thickness distribution and stringer areas in the initial barrel configuration (upper row) and the barrel mass during the SOL200 iteration (middle row). For the optimised barrel (lower row) the skin thickness and stringer areas.

whole barrel) rather than by the constraints for optimum skin thickness and stringer area. Therefore an additional GFEM barrel optimisation is performed with decreased lower bounds of the design variables where the minimum values of both skin and stringer thicknesses are decreased to 1·0mm.

Because of the decrease of the lower bounds of the skin thickness and stringer cross-sectional area in the barrel optimisation, it is also required to decrease the lower bounds in the panel optimisations. Therefore the DOE set for the panel analyses are extended to the lower bounds by adding for skin thickness and stringer thickness values down to 1·0mm. This results in a total additional DOE set of 12,320 design points for all the considered variables for each of the two stringer pitches, yielding a total data set of (24,640 + 12,320) x 2 data points. The surrogate models of the panel buckling loads ($\tilde{\lambda}_{sk}$, $\tilde{\lambda}_{gl}$, $\tilde{\lambda}_{fr}$) are regenerated with this extended data set. Then

https://doi.org/10.1017/S0001924000008915 Published online by Cambridge University Press

the panel optimisations again are executed and the surrogate models of the optimised global skin thickness ($\tilde{t}_{skgopt}(\theta, \varphi, F)$) and optimised global stringer cross sectional area ($\tilde{A}^{p}_{skgopt}(\theta, \varphi, F,)$ are regenerated. These extended surrogate models of the optimum global variables are then applied in the updated GFEM barrel optimisation. The initial values of the design variables are set to the optimum values found in the previous optimisation, i.e. 1·6mm for skin thickness and 101mm^2 for stringer cross sectional area with initial total barrel mass of 1,226kg. The lower and upper bounds of the design variables are set to 1·0mm and 8·0mm for skin thickness and 70mm^2 and 457mm^2 for stringer cross sectional area.

The SOL200 solution now requires five major iterations to achieve the final optimum. The total mass of the optimum barrel design has decreased from 1,225kg to 1,157 kg (about 5% improvement). In the optimised barrel now the skin thickness and stringer areas decreased to their optimum values as prescribed by the constraints, and remain clearly above the lower bounds. Consequently this optimisation is driven by the constraints for optimum skin thickness and stringer area (in large portions of the barrel) rather than by the lower bounds of the design variables.

9.0 CONCLUSIONS

This paper presents an innovative optimisation procedure for large aircraft fuselage structures based on FEM analyses. The local level FEM analyses have several advantages (like generic implementation, based on public commercial analysis tools, allow for detailed modelling and analysis), but require substantial computational cost. Computational efficiency is achieved by exploitation of advanced surrogate models and optimisation algorithms. The global level optimisation includes only variables and constraints in certain design regions of the barrel model. This simplification is used under the assumption that the structures in the other regions of the barrel (window belt, door surround, floor structures) have been sized with sufficient stiffness and strength in the preliminary sizing process. But to ensure no failure in these other regions the constraints should actually also be evaluated in these regions.

10.0 DISCUSSION OF MODELLING ASPECTS

Failure criteria: The present study is limited to only buckling criteria. The panel level analyses and optimisations could be further extended to include other detailed failure criteria (e.g. strength, damage tolerance, etc.), which would then appear as additional constraint functions in the panel level optimisations and would be rather straight-forward to implement. Of course the additional panel level analyses would require extra computational effort.

Post-buckling: The present study is limited to linear buckling analysis. Non-linear post-buckling analyses could be used instead but are presently out of scope. Besides the dramatic increase in computation time of the panel level analyses, also the evaluation of adequate buckling values for the panel would become significantly more complex. Therefore we recommend to stick to linear panel buckling analyses and only use post-buckling for validation assessments of (small) sub-sets of the linear buckling results.

Composites: Composite laminate properties were properly modelled in the panel and barrel FE models, but were not specifically included as design variables. Nevertheless these properties were included in a simplified way as proportional ply thicknesses in the skin and stringers of the panel DFEM model. Variable composite lay-ups could be included in the optimisation procedure. However, a complete combinatorial representation of all possible stacking sequences of skin and

https://doi.org/10.1017/S0001924000008915 Published online by Cambridge University Press

stringers in the panel level optimisations would strongly increase the computational effort of the panel level optimisations, especially if large laminate thicknesses (i.e. many plies) should be allowed.
Optimum variables: the given approach yields fixed combinations of optimised local design variables. On the local level that is adequate, but on the global level it would be preferable if the global-local constraints (i.e. here related to the buckling criteria) that are applied to the global design variables were more independent. That could allow for example for some relaxation on one variable and some restriction on the other, which could lead to a superior global optimum. This might be achieved by attaining Pareto sets of non-dominated design on the local level, but it would need further investigation on what objectives and constraints should then be applied in the lower level optimisations.
Post-identification: although the global level optimisation yields only the final global design variables, the local sizing variables (in particular, the stringer variables) can be retrieved by local level assessment, i.e. by executing the local level optimisation for the internal loadings in the optimised barrel model. For better accuracy, first the surrogate models of the buckling loads could be improved by evaluating the DFEM analysis for these internal loading conditions.

11.0 DISCUSSION OF COMPUTATIONAL ASPECTS

Accuracy: It is difficult to achieve surrogate models of the panel buckling behaviour with sufficient accuracy. The accuracy can be improved by using denser DOE sampling, i.e. more (expensive) DFEM evaluations, and better surrogate modelling methods. Similarly, the accuracy of the surrogate models of the optimum panel level variables can be further improved by denser DOE sampling, i.e. by running the panel level optimisations in more loading conditions. These panel level optimisations can be run very efficiently (around 1 s on standard PC) thanks to the previously generated surrogate models of the panel buckling behaviour.

Global-local iteration: although the initial accuracy of the surrogate models is not very high, the procedure does allow to adaptively improve this accuracy by feeding the internal loads after each barrel level optimisation into the panel level analyses and optimisations, yielding additional DFEM analysis results in the data base for the local level surrogate models. This adaptive surrogate modelling process can yield (locally) accurate but cheap surrogate models.

Gradients: in the panel level optimisations the analytical gradients of the objective function and of the surrogate models for the constraint functions could be exploited, but are not used here because of the implementation effort and the limited gain in time (few seconds or less) that could be achieved. In the global level optimisation the analytical gradients of the surrogate models for the optimum global variables are available, but could not be exploited because the gradients of the DRESP3 variables could not be applied in the NASTRAN version that is used (MSC NASTRAN R2005.5).

Design variables: The panel level optimisations consider only a limited number of detailed sizing variables. Of course more variables could be considered but would require proportionally more computational effort on the panel level.

ACKNOWLEDGEMENTS

The research leading to these results has received funding from the European Community's Seventh Framework Programme FP7/2007-2013 under grant agreement n°213371 (MAAXIMUS, www.maaximus.eu).

https://doi.org/10.1017/S0001924000008915 Published online by Cambridge University Press

REFERENCES

1. KASAPOGLOU, C. *Design and Analysis of Composite Structures: With Applications to Aerospace Structures*, 2010, Wiley.
2. GRIHON, S., KROG, L. and BASSIR, D. Numerical optimisation applied to structure sizing at AIRBUS: A multi-step process, *Int J Simul Multidisci Des Optim*, 2009, **3**, pp 432-442.
3. HAFTKA, R.T. and GÜRDAL, Z. *Elements of Structural Optimisation*, 1992, Springer.
4. SOBIESZCZANSKI, J. and LOENDORF, D. A mixed optimisation method for automated design of fuselage structures. *J Aircr*, 1972, **9,** (12), pp 805-811.
5. SOBIESZCZANSKI-SOBIESKI, J., JAMES, B. and DOVI, A. Structural optimization by multilevel decomposition, *AIAA J*, 1985, **3**, pp 124–142.
6. SOBIESZCZANSKI-SOBIESKI, J., JAMES, B. and RILEY, M. Structural sizing by generalized, multilevel optimization, *AIAA J*, 1987, **25**, pp 139–145.
7. BEERS, M. and VANDERPLAATS, G. A linearization method for multilevel optimization, 1987, International Conference on Numerical Methods in Engineering: Theory and applications, Swansea, Martinus Nijhoff Publishers.
8. BARTHELEMY, J.F.M. and SOBIESZCZANSKI-SOBIESKI, J. Optimum sensitivity derivatives of objective functions in nonlinear programming, Technical notes, 1983, AIAA.
9. SOBIESZCZANSKI-SOBIESKI, J. A step from hierarchic to non-hierarchic systems, 1988, Second NASA Air Force Symposium on recent advances in multidisciplinary analysis and optimization.
10. SOBIESZCZANSKI-SOBIESKI, J. Sensitivity of complex, internally coupled systems, *AIAA J*, 1990, **28**, (1), pp 153–160.
11. HUTCHISON, M.G., UNGER, E.R., MASON, W.H., GROSSMAN, B. and HAFTKA, R.T. Variable-complexity aerodynamic optimization of a high-speed civil transport wing, *J Aircr*, 1994, **31**, (1), pp 110-116.
12. BURGEE, S., GIUNTA, A.A., BALABANOV, V., GROSSMAN, B., MASON, W.H., NARDUCCI, R., HAFTKA, R.T. and WATSON, L.T. A coarse-grained parallel variable-complexity multidisciplinary optimization paradigm, *Int J High Performance Computing Applications*, 1996, **10**, (4), pp 269-299.
13. SHANKAR, J. RIBBENS, C. HAFTKA, R. and WATSON, L. Computational study of a non-hierarchical decomposition algorithm, *Computational Optimization and Applications*, 1993, **2**, pp 273–293.
14. RENAUD, J. A and ND GABRIELE, G. Approximation in non-hierarchic system optimization, *AIAA J*, 1994, **32**, pp 198–205.
15. RODRÍGUEZ, J., RENAUD, J. and WATSON, L. Convergence of trust region augmented Lagrangian methods using variable fidelity approximation data, *Structural Optimization*, 1998, **15**, pp 141–156.
16. PAIVA, R.M., CARVALHO, A.R.D., CRAWFORD, C. and SULEMAN, A. Comparison of surrogate models in a multidisciplinary optimization framework for wing design, *AIAA J*, 2010, **48**, (5), pp 995-1006.
17. BETTEBGHOR, D. Optimisation Biniveau de Structures Aeronautiques Composites, 2011 PhD thesis, Doctorat de l'université de Toulouse, France,.
18. COLSON, B., BRUYNEEL, M., GRIHON, S., JETTEUR, PH., MORELLE, P. and REMOUCHAMPS, A. Composite panel optimization with nonlinear finite-element analysis and semi-analytical sensitivities, 2007, NAFEMS Seminar on Simulating Composite Materials and Structures, 6-7 November 2007, Bad-Kissingen, Germany.
19. FLEURY, C., BRUYNEEL, M., COLSON, B. and REMOUCHAMPS, A. Buckling optimization of composite stiffened panels: some important issues, 2010, Second ICEO, September 2010, Lisbon, Portugal.
20. VANKAN, W.J., LAMMEN, W.F. and MAAS, R. Meta-modeling and multi-objective optimization in aircraft design, *Advances in Collaborative Civil Aeronautical Multidisciplinary Design Optimization*, Ch 6, KESSELER, E. and GUENOV, M. (Eds), 2010, AIAA, (NLR-TP-2009-718).
21. SIMPSON, T.W., PEPLINSKI, J.P., KOCH, P.N. and ALLEN, J.K. Metamodels for computer-based engineering design: survey and recommendations, *Engineering with Computers*, 2001, **17**, pp 129-150, .
22. BETTEBGHOR, D. and BARTOLI, N. Approximation of the critical buckling factor for composite panels, *Structural and Multidisciplinary Optimization*, 2012, **46**, (4), pp 561-584.
23. MSC Software, MSC NASTRAN http://www.mscsoftware.com/products/cae-tools/msc-nastran.aspx (accessed 4-7-2012).
24. Dassault Systèmes Simulia, http://www.3ds.com/products/simulia/portfolio/abaqus/overview/ (accessed 4-7-2012).
25. The Mathworks, http://www.mathworks.nl/products/matlab/ (accessed 4-7-2012).

https://doi.org/10.1017/S0001924000008915 Published online by Cambridge University Press